Nils G. Walter
Dinari A. Harris
Miguel J. B. Pereira
David Rueda
Department of Chemistry,
The University of Michigan,
930 N. University,
Ann Arbor, MI 48109-1055

In the Fluorescent Spotlight: Global and Local Conformational Changes of Small Catalytic RNAs

Received 22 January 2002;
accepted 22 January 2002
Published online 25 April 2002 in Wiley InterScience (www.interscience.wiley.com). DOI: 10.1002/bip.10144

Abstract: *RNA is a ubiquitous biopolymer that performs a multitude of essential cellular functions involving the maintenance, transfer, and processing of genetic information. RNA is unique in that it can carry both genetic information and catalytic function. Its secondary structure domains, which fold stably and independently, assemble hierarchically into modular tertiary structures. Studies of these folding events are key to understanding how catalytic RNAs (ribozymes) are able to position reaction components for site-specific chemistry. We have made use of fluorescence techniques to monitor the rates and free energies of folding of the small hairpin and hepatitis delta virus (HDV) ribozymes, found in satellite RNAs of plant and the human hepatitis B viruses, respectively. In particular, fluorescence resonance energy transfer (FRET) has been employed to monitor global conformational changes, and 2-aminopurine fluorescence quenching to probe for local structural rearrangements. In this review we illuminate what we have learned about the reaction pathways of the hairpin and HDV ribozymes, and how our results have complemented other biochemical and biophysical investigations. The structural transitions observed in these two small catalytic RNAs are likely to be found in many other biological RNAs, and the described fluorescence techniques promise to be broadly applicable.* © 2002 Wiley Periodicals, Inc. Biopoly (Nucleic Acid Sci) 61: 224–241, 2002

Keywords: *fluorescence quenching; fluorescence resonance energy transfer; folding free energy landscape; ribozyme; RNA folding kinetics*

INTRODUCTION

Nature uses fundamental principles of organic and physical chemistry to generate self-replicating and evolving biopolymers that make up life as we know it. In this respect, RNA is a particularly well-suited biopolymer with a unique ability to carry both genetic information and catalytic function. It plays a key role in all aspects of the maintenance, transfer, and processing of genetic information, in the form of messenger, transfer, ribosomal, spliceosomal RNAs, and viral RNA genomes. According to the RNA World hypothesis, it may even have initiated life on earth.[1] Only recently, we have begun to discover some of the reasons for this central function. First, RNA serves a role in the coding and decoding of genetic information through specific Watson–Crick base pairing (secondary structure). Second, RNA forms catalytically active

Correspondence to: Nils G. Walter; email: nwalter@umich.edu
Contract grant sponsor: NIH
Contract grant number: GM62357

components of the gene processing machinery through folding into intricate tertiary structures with precisely positioned unpaired nucleobases. Finally, RNA can undergo substantial conformational changes in the course of a reaction pathway without the need for an external energy source through its intrinsic structural dynamics. In the extreme, the same RNA sequence may fold into two entirely different secondary and tertiary structures with distinct catalytic activities.[2]

The number of confirmed naturally occurring catalytic RNAs, or ribozymes, is continuously on the rise. The most recent count includes the ribosomal RNAs of the protein biosynthetic machinery[3] and the small nuclear RNAs of the eukaryotic splicing machinery.[4] For these large ribonucleoprotein complexes, activity of the RNA in the absence of protein components is slow and rudimentary,[4,5] yet undoubtedly the RNA carries the functional components for catalysis. The role of the proteins seems to be limited to helping align RNA catalytic core components and substrates, and to timing the multitude of conformational rearrangements that lead to a full catalytic cycle.[6,7]

Even including the most recent recruits among the naturally occurring ribozymes, their organic chemistry repertoire is limited to nucleophilic substitutions on phospho or carboxyl esters, either with internal (*"cis"*) or external (*"trans"*) substrates. This limitation contrasts with the multitude of catalytic functions of protein enzymes. It is at least in part imposed by the limited diversity of functional groups on the four basic nucleotide building blocks of RNA, compared to the twenty amino acids of proteins. This restriction in chemical capacity has been partially lifted by artificial in vitro selection of ribozymes with activities such as glycosidic bond hydrolysis and Diels–Alder cycloaddition, but for a still broader catalytic range the incorporation of additional functional moieties appears necessary.[8] Interestingly, there is no evidence that nature has expanded its catalytic repertoire by making use of the 95 modified nucleosides known to occur in natural RNA.[9,10] In recent years it has become clear that, by precisely positioning the nucleobases A, U, G, and C, and other reaction components in the catalytic core, RNA can lower the activation barrier for site-specific chemistry by employing metal ion catalysis, general acid–base catalysis by nucleobases with electrostatically modulated pK_a, and intrinsic substrate binding energy.[11,12]

The catalytic repertoire of the subclass of four naturally occurring small ribozymes is restricted to the same reversible phosphodiester transfer reaction that occurs spontaneously in base-catalyzed chemical RNA degradation. Yet the hammerhead, hairpin, hepatitis delta virus (HDV), and *Neurospora* Varkud satellite (VS) ribozymes accelerate this reaction by six to seven orders of magnitude and lend it site specificity, which characterizes them as true catalysts. All four ribozymes were isolated from small self-replicating satellite RNAs. They are assumed to play a crucial role in the double-rolling circle replication of these satellite RNAs, acting as a site-specific endonuclease and ligase in different stages of replication. In case of the hammerhead, hairpin, and HDV ribozymes, their particularly small size (<85 nucleotide (nt)) has enabled chemical synthesis and detailed structural and enzymologic studies. We now have atomic-resolution crystal structures available to provide a framework for probing into their dynamics and function (for a recent review, see Ref. 13). For the somewhat larger VS ribozyme (160 nt), which so far has eluded crystallization attempts (R. Collins, personal communications), information on the location of the catalytic core has recently emerged.[14,15]

Nature's solutions to accomplish site-specific RNA backbone cleavage are surprisingly diverse; that is, the secondary and tertiary structures of the four small ribozymes are very distinct from one another. This is surprising since in vitro selection from an unbiased random RNA pool nearly exclusively yields only the simplest of these motifs, the hammerhead ribozyme.[16] The reason for nature to choose among different, more complex solutions may lie in specific requirements for the double-rolling circle replication of a particular satellite RNA. For example, timing of cleavage and ligation in different replication stages may require regulated folding and unfolding of the active structure; or requirements such as stability against host cellular ribonucleases, compatibility with viral packaging, or the necessity to have a catalytically active motif in both complementary strands may impose specific sequence restrictions on the motifs to be used in each satellite RNA.

By comparison to their limited organic chemistry repertoire, ribozymes have started to amaze us with a rich physical chemistry of folding into their functional structures. The high thermodynamic stability of base pairs (through both hydrogen bonding and base stacking) provides the basis for folding of proximal, partially self-complementary regions into domains with secondary structure.[17,18] Recent work has provided evidence for a hierarchical assembly of these independently and stably folded domains into larger modular RNA structures (reviewed in Refs. 19 and 20). To accommodate distal tertiary interactions, local interactions often have to be broken and rearranged. Such processes can pose kinetic traps for folding into the

functional (native) structure,[21] providing for rugged folding free energy landscapes.[22,23] Studies of these folding events are key to understanding how catalytic RNAs are able to position reaction components so that they are poised for site-specific chemistry.

We have made use of fluorescence techniques to monitor the rates and free energies of folding of several small catalytic RNAs into functional structures. Although these studies are certainly not limited to catalytic RNA, ribozymes provide convenient model systems as their catalytic function readily reports the presence of a fully folded native structure. In particular, we have studied the hairpin ribozyme, derived from the negative strand of the tobacco ringspot virus satellite RNA, and the HDV ribozyme found in the human pathogen HDV. In this review we illuminate what we have learned from these studies about global and local conformational rearrangements along the reaction pathway, and how our results have complemented other biochemical and biophysical investigations. We have organized the text by ribozyme, and in both cases present data from steady-state fluorescence resonance energy transfer (FRET), time-resolved FRET, and 2-aminopurine fluorescence quenching.

THE HAIRPIN RIBOZYME

The hairpin ribozyme is a small endonucleolytic RNA motif of ~50 nucleotides that has proven to be an exciting model for RNA folding problems[21,24–29] as well as a promising gene therapeutic agent for targeted RNA inactivation.[29,30] From the naturally occurring RNA four-way junction, it has been engineered into a hinged two-way junction that cleaves external substrates in *trans* immediately 5′ of G+1.[27] This minimal ribozyme–substrate complex consists of the two helix–loop–helix domains A and B. A number of studies, including those reviewed here, have revealed the multistep reaction pathway shown in Figure 1a: (1) substrate S binds to the ribozyme forming an extended and inactive conformation, in which domains A and B are coaxially stacked; (2) the complex folds into an active docked conformation with the two domains interacting side-by-side; (3) reversible cleavage occurs; (4) the complex undocks and the cleavage products dissociate or vice versa. High-resolution NMR structures of the isolated domains A[31] and B[32] have been determined, and their base pair interactions are summarized in the extended conformation of Figure 1a. Aside from the fluorescence techniques outlined below, docking has been studied by hydroxyl-radical footprinting,[26] interdomain cross-linking,[33–35] and molecular modeling.[33,35,36] Regarding specific interactions between the two domains in the docked structure, mutational analyses have revealed a functionally crucial Watson–Crick base pair between G+1 of the substrate and C25 of the ribozyme core.[36] In a recent crystal structure of the hairpin ribozyme,[37] this base pair as well as several additional hydrogen bonds, including a ribose zipper motif first predicted by modification interference[38,39] and modeling studies,[33] were identified as the network of contact points responsible for domain docking (all summarized in the docked conformation of Figure 1a). In the crystal structure, G+1 is inserted into a highly complementary binding pocket in domain B, highlighted in Figure 1b. The accompanying base flipping of G+1 generates the backbone in-line attack configuration required for site-specific S_N2-type phosphodiester cleavage chemistry immediately 5′ of G+1. It has been noted how nicely the crystallographic, biochemical, and computational studies of the hairpin ribozyme have complemented each other in correlating structure and function.[40]

Studies of its metal ion dependence revealed a fascinating feature of the hairpin ribozyme in that it does not employ divalent metal ions as obligatory catalytic components during reaction chemistry.[41–43] This discovery ran contrary to previous belief in the field,[44] and sparked renewed interest in dissecting the roles of metal ions in folding and function of small catalytic RNAs. This enhanced interest led, in turn, to the surprising finding that all small catalytic RNAs are functional in monovalent cations alone,[45–47] providing direct evidence that the RNAs themselves carry all catalytic residues. To explain how a linear RNA chain can form the scaffold that positions all these components for catalytic function, probing into the folding of its three-dimensional structure becomes particularly important. In case of the hairpin ribozyme, fluorescence methods have turned out to be ideally suited to probe into the kinetics and thermodynamics of folding.

Domain Docking of the Hairpin Ribozyme is Revealed by Steady-State FRET

FRET, or Förster transfer,[48] originates from the nonradiative dipole–dipole interaction of two fluorophores, called donor and acceptor, through space.[49–59] The resulting strong dependence of the energy transfer rate k_T and hence the energy transfer efficiency E_T on the donor–acceptor distance R is expressed as

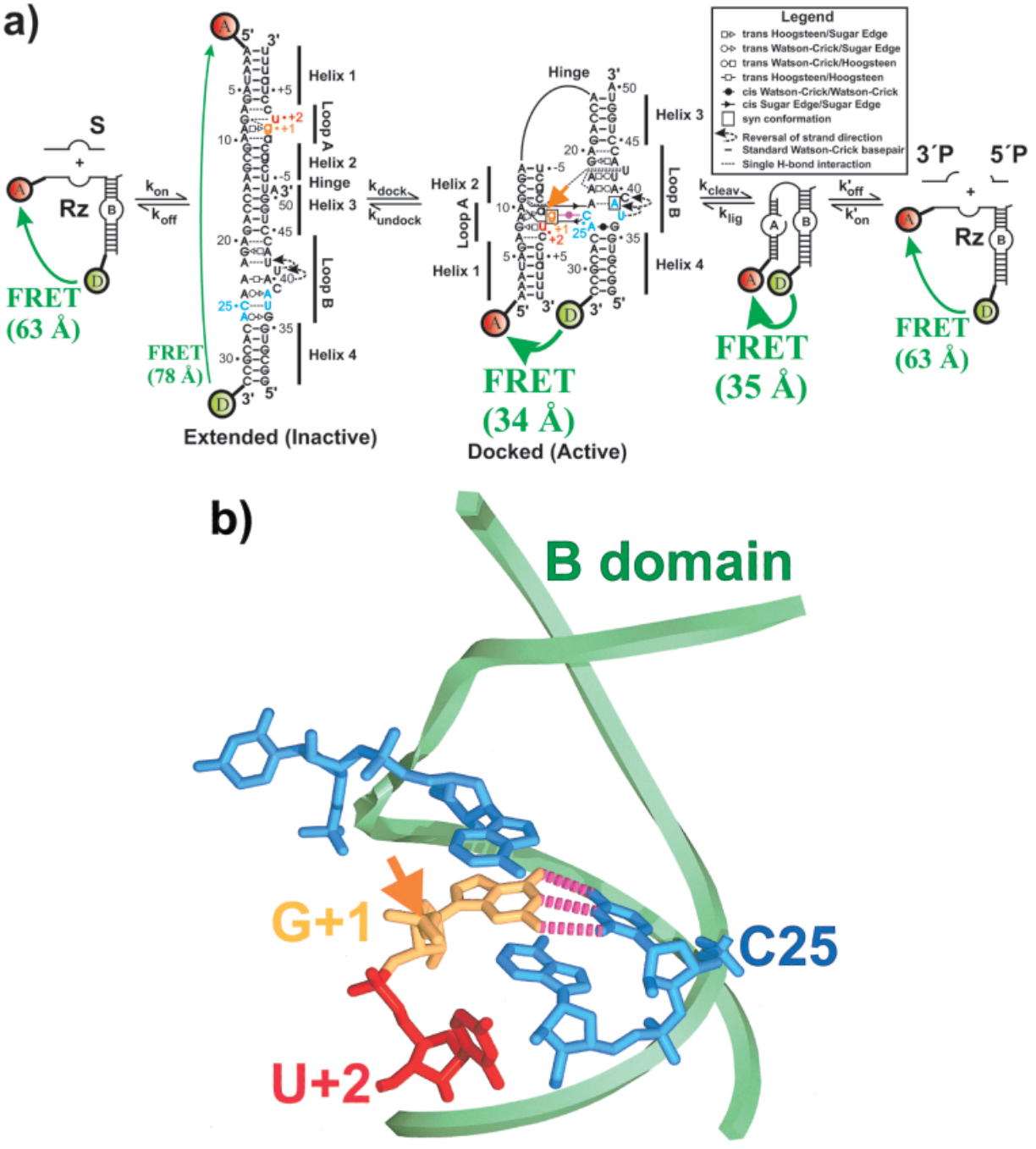

FIGURE 1 Catalysis by the hairpin ribozyme. (a) Schematic of the minimal reaction pathway of the hairpin ribozyme. Substrate (S) is bound by the ribozyme (Rz) to form an extended complex, with helices 2 and 3 coaxially stacked. This inactive intermediate needs to bend around a flexible hinge for loops A and B to interact in the docked, active conformation. For both the extended and docked conformers we use a two-dimensional representation, annotated according to Ref. 85 with their tertiary structures as suggested by NMR[31,32] and x-ray crystallography,[37] respectively; the colored nucleotides and base-pair interaction are the ones detailed in (b). The cleaved docked complex presumably partitions between re-ligation of the cleavage products and undocking. The short 5′ and 3′ products (5′P, 3′P) then dissociate from the complex. (b) Details of the catalytic core. G+1 of the substrate is held in place by a Watson–Crick hydrogen-bonding interaction (dashed tubes) with C25 of the ribozyme B domain (green ribbon, backbone), flipping the base so that an in-line attack configuration is reached at the cleavage site (arrow). U+2 unstacks from G+1 as a result of an induced fit upon domain docking. This figure was generated using the crystal structure[37] and Swiss-PdbViewer 3.7.[86]

$$k_T = \frac{1}{\tau_D}\left(\frac{R_0}{R}\right)^6 \quad (1)$$

and

$$E_T = \frac{R_0^6}{R^6 + R_0^6} \quad (2)$$

where τ_D is the donor fluorescence lifetime in the absence of acceptor and R_0 is the Förster distance at which E_T is 50%. R_0 is dependent on the spectral overlap and the relative spatial orientation of the utilized fluorophores, and typically has a value of 20–90 Å, which enables the measurement of fluorophore distances in the range of 10–100 Å. When two fluorophores are covalently tethered to defined sites on a biopolymer, or on two molecules in a complex, the distance between these sites can be measured. The distance range accessible by FRET is ideal for many biological macromolecules and fills the gap between that of other techniques, such as NMR and cryo electron microscopy (see also other articles in this issue). In addition, changes in fluorophore distance over a biopolymer folding time course can be monitored in real time under a wide variety of buffer conditions when continuously exciting the donor (steady-state excitation).

To enable steady-state FRET (ss-FRET) measurements between domains A and B of the hairpin ribozyme, we have utilized a synthetically convenient fluorescein–hexachlorofluorescein donor–acceptor pair on the 3′ and 5′ ends, respectively, of the 5′ segment of the ribozyme (Figure 1a) (for specifics on labeling chemistry, see Refs. 24 and 58). We have found that other donor–acceptor pairs such as fluorescein–tetramethylrhodamine or Cy3–Cy5 yield very similar results. A 10-fold molar excess of the separate 3′ segment is annealed to the 5′ segment in standard buffer (50 m*M* Tris HCl, pH 7.5, 12 m*M* $MgCl_2$, 25 m*M* dithiothreitol (DTT), and at 25°C) to ensure that the fluorescently labeled strand is quantitatively converted into assembled ribozyme. The sequences of ribozyme and substrate are optimized for rapid substrate binding and efficient catalysis.

Upon mixing of the fluorophore-labeled ribozyme with a 10-fold excess of cognate noncleavable substrate analog S(2′OMeA-1), in which the nucleophilic 2′ OH group of A-1 is replaced by a 2′ O-methyl group to block the cleavage reaction, an instant acceptor quench and slight donor dequench are observed (Figure 2).[24] A concomitant fluorescence anisotropy increase of the acceptor reveals the decreasing fluorophore mobility upon substrate binding, which, under the utilized conditions, is fast and occurs within the manual mixing time.[60] Noncognate substrates do not lead to any of these changes. From these observations we conclude that the instant fluorescence changes upon cognate substrate addition are due to, first, quenching of hexachlorofluorescein, and second, decreased FRET between donor and acceptor in the extended conformation adopted by the ribozyme–substrate complex.[24]

Subsequently, the donor fluorescence decreases over several minutes, while the acceptor fluorescence increases at the same rate (Figure 2). This observation strongly suggests that the underlying molecular process involves increasing FRET between the two fluorophores, as expected for their approach upon domain docking in the ribozyme–substrate complex (inset of Figure 2). From the temporal change of the ratio $Q = F_{560}/F_{515}$, a relative measure of the FRET efficiency, the rate constant of the transition between the extended and docked conformations is extracted.[24] For the reversible docking step of the noncleavable substrate analog, the observed docking rate constant $k_{dock,obs}$ of (0.84 ± 0.04) min^{-1} is a combination of the elementary docking and undocking rate constants:

$$k_{dock,obs} = k_{dock} + k_{undock} \quad (3)$$

The $k_{dock,obs}$ can only be further dissected by an independent measurement of the docking equilibrium constant or the undocking rate constant. A fraction of 61% docked ribozyme–substrate analog [S(2′OMeA-1)] complex, measured by time-resolved FRET (see section on global geometry and equilibrium position below),[25] leads to estimates for k_{dock} and k_{undock} of 0.5 and 0.3 min^{-1}, respectively. A cleavable all-ribose substrate with 2′ hydroxyl group on A-1 yields very similar rate constants when considering that the observed docking rate constant $k_{dock,obs}$ of (1.02 ± 0.07) min^{-1} also contains the rate of cleavage:

$$k_{dock,obs} = k_{dock} + k_{undock} + k_{cleav} \quad (4)$$

The k_{cleav} has a value of 0.14 min^{-1} under these conditions. That makes docking into an active ribozyme–substrate complex about 3.5 times faster than cleavage and, therefore, only partially rate limiting.[24] Interestingly, when A-1 is modified to 2′ deoxy [in the noncleavable substrate analog S(dA-1)], the observed rate constant $k_{dock,obs}$ of (0.64 ± 0.04) min^{-1} is slightly slower than with a 2′ O-methyl or 2′ hydroxyl. Perhaps this observation reflects the different sugar pucker preference of 2′ deoxy (C2′-*endo*) compared to either 2′ O-methyl or 2′ hydroxyl (C3′-

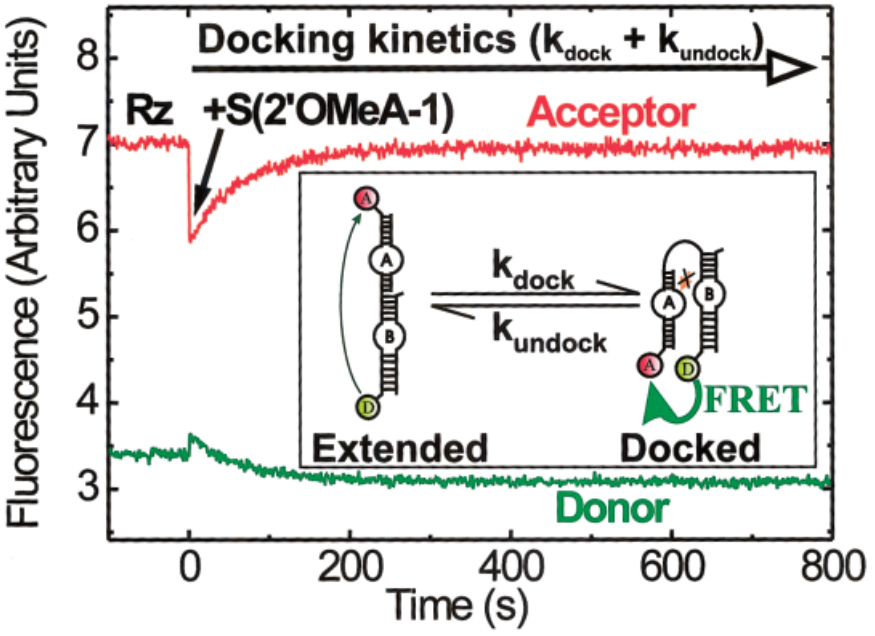

FIGURE 2 Analysis of the docking kinetics of the hairpin ribozyme–substrate complex by ss-FRET. The doubly labeled ribozyme displays a strong signal for the acceptor fluorophore and a weaker one for the donor. Upon manual addition of a tenfold excess of noncleavable substrate analog [S(2′OMeA-1)], significant quenching of the acceptor fluorescence is observed due to rapid ribozyme–substrate complex formation. Subsequently, the acceptor signal increases, while the donor signal decreases at the same rate, revealing the reversible docking kinetics from an extended to a docked conformation (inset: green arrow, FRET; crossed-out arrow, substrate modification to render it noncleavable). Standard conditions: 50 m*M* Tris HCl, pH 7.5, 12 m*M* $MgCl_2$, at 25°C.

endo),[61] or its lack of a hydrogen bond with G+8,[37] which may, in turn, impact the ability to promote base flipping of the adjacent G+1 as required for access to the docked conformation.[37]

Strikingly, most modifications to the RNA sequence or reaction conditions that inhibit catalysis do so by interfering with docking.[24] For example, substitution of G+1 with A, C, or U results in profound inhibition of the reaction.[62] Use of the G+1A mutant in the ss-FRET assay proves that the modified substrate indeed binds to the substrate-binding strand, as indicated by quenching of hexachlorofluorescein (see above). However, no subsequent increase in FRET is observed. Therefore, we can conclude that the mechanism of inhibition by a G+1A substitution involves blocking of the essential domain docking step, and not direct interference with reaction chemistry as suggested previously.[62] When a compensatory mutation, C25U, is introduced into domain B, catalytic activity is restored to within 10-fold of wild-type activity, although docking is still not observable.[36] In general, all Watson–Crick-type combinations between the substrate +1 and ribozyme 25 positions show such a behavior, which for the first time proved a functionally important interaction between these positions. This crucial interaction was later confirmed in the crystal structure of the hairpin ribozyme.[37] In the partially active double mutants, such as G+1A/C25U, domain docking is less stable and transient, as recently observed by single-molecule FRET.[87]

For substrate variants with U+2 substitutions that result in a 70- to 13-fold reduced cleavage activity domain, docking is generally stable.[63] Interestingly, the FRET signal increase clearly displays a second, slower phase, a unique feature among all tested modifications of sequence or conditions.[24] This second phase leads to a higher overall amplitude of the FRET increase that can be correlated with a higher abundance of docked complex. This observation invokes a mechanism of functional interference by a U+2 mutation in which the ribozyme–substrate complex becomes trapped in a native-like docked fold, proceeding only slowly to the transition state[63] (see also section on local structural dynamics below). Recently, similar evidence has been invoked to suggest a direct catalytic role of G+8 in reversible cleavage chemistry.[64]

We further have used ss-FRET to compare domain docking under a variety of ionic conditions. As expected, divalent metal ions that promote catalytic ac-

tivity, such as Mg^{2+}, Ca^{2+}, or Sr^{2+}, lead to efficient docking, the rate of which increases with the (millimolar) cation concentration.[24] High ($>1M$) concentrations of monovalent cations, such as Na^{+}, also promote both docking and cleavage.[45] These results support the notion that metal ions are not obligatory chemical participants in the reaction catalyzed by the hairpin ribozyme, but rather assist and accelerate folding of the RNA into the active docked conformation by neutralizing negative backbone charges.[27] Based on crystallographic and biochemical evidence, G+8 and A38 have recently been proposed to then become positioned to contribute the functional groups necessary for general acid–base catalysis of reversible cleavage.[37,64]

Our results demonstrate the versatility of ss-FRET to directly monitor global RNA folding events in solution under a variety of conditions and to derive RNA folding kinetics. Analyses using time-resolved FRET perfectly complement these data by providing information on the relative stability and the structural characteristics of the conformers involved.

Global Geometry and Equilibrium Position of Domain Docking are Derived from Time-Resolved FRET

While steady-state FRET enables detection of qualitative structural changes, it does not allow us to quantify their magnitude. To measure absolute distances between the fluorophores attached to the hairpin ribozyme, we employed time-resolved FRET (tr-FRET). Figure 3 shows the principle of these measurements. The hairpin ribozyme is doubly labeled with a donor (fluorescein) and an acceptor fluorophore (tetramethylrhodamine) whose emission maxima are well separated so that the donor emission can be optically isolated. First, the time-resolved donor fluorescence decay in a donor-only labeled ribozyme–substrate complex is measured. Then, the donor fluorescence decay in the donor–acceptor doubly labeled complex is measured under identical conditions. The faster decay in the doubly labeled ribozyme is due to FRET from donor to acceptor; the closer the two fluorophores are the shorter the donor fluorescence lifetime. On the time scale of a typical donor fluorophore lifetime in the excited state (nanoseconds), large-scale molecular motions are slow and the donor–acceptor distance appears fixed. Therefore, each individual donor–acceptor distance will be characterized by a unique donor fluorescence lifetime. A flexible molecule will display a distribution of donor–acceptor distances that projects into a distribution of donor lifetimes. If, as is the case for the hairpin ribozyme, there are two distinct conformational isomers in equilibrium, each one will contribute its specific donor lifetime distribution that can be discerned in the overall fluorescence decay (Figure 3).[25] The principle of the tr-FRET method and details of the instrumentation and data analysis are described in the accompanying article by Klostermeier and Millar.

It is important to note that the single-photon counting techniques used to obtain the high-precision decay data require a significant acquisition time of tens of minutes. Hence, only samples in thermodynamic equilibrium can be studied. "Time-resolved" FRET refers to the fact that fluorescence decay data are measured, while the distance distribution(s) need to remain constant over the data acquisition time. In contrast, ss-FRET allows one to derive kinetic data (see section immediately above).

Application of the tr-FRET methodology to the wild-type hairpin ribozyme with bound S(dA-1) substrate analog reveals two distinct lifetime and distance distributions, corresponding to docked and extended conformers (Figure 3). Thus, tr-FRET resolves the equilibrium distribution between the two hairpin ribozyme conformational isomers in solution (Figure 3). Under standard conditions, 65% of the wild-type ribozyme–substrate analog [S(dA-1)] complex resides in the active docked conformation with a mean donor–acceptor distance of 34 Å (full-width-at-half-maximum, fwhm, 18 Å), while 35% of the population adopts the inactive extended conformation with a mean distance of 78 Å (fwhm, 18 Å). In contrast, the G+1A mutant ribozyme–substrate complex is best described by a single, extended conformation, as predicted by our ss-FRET experiments. It is important to note that other methods that yield RNA structural information, such as NMR, x-ray crystallography, or chemical probing techniques, often fail to do so on conformer mixtures. By contrast, tr-FRET extracts mean distances between the donor–acceptor labeling sites on the extended and docked hairpin ribozyme conformers, useful for molecular modeling purposes, and quantifies their relative abundance at equilibrium.[25] The latter values define the equilibrium constant for docking K_{dock}:

$$K_{dock} = \frac{\text{Docked Fraction}}{\text{Undocked Fraction}} = \frac{k_{dock}}{k_{undock}} \qquad (5)$$

Together with Eq. (3) and the kinetic data derived from ss-FRET, the elementary docking and undocking rate constants k_{dock} and k_{undock} are deduced (0.5 and 0.3 min^{-1}, respectively, see section immediately above). In addition, the associated free energy differ-

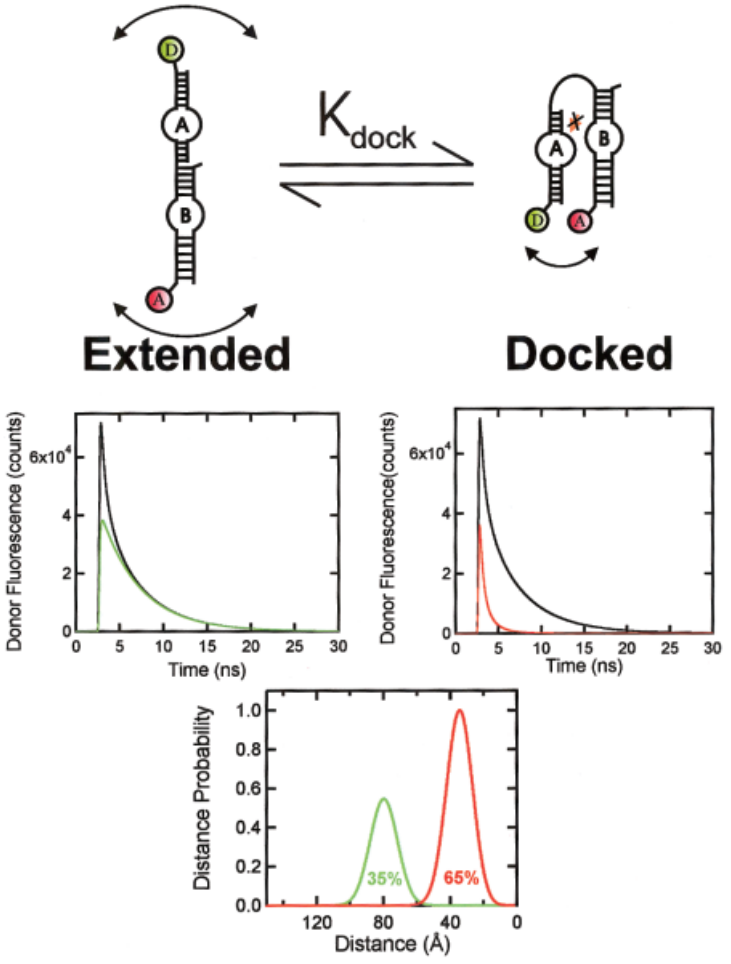

FIGURE 3 Top, revealing the equilibrium between the extended and docked conformers of the hairpin ribozyme by tr-FRET. For these studies, a noncleavable substrate analog is employed, indicated by the crossed-out arrow. Middle, the donor decay data (black line) can only be fit assuming lifetime contributions from two Gaussian donor–acceptor distance distributions, revealing the presence of both extended (green contribution) and docked conformers (red contribution). Bottom, the relative abundance of these isomers is directly obtained from the analysis and is reflected in the relative peak areas of the corresponding distance distributions. Conditions: 50 m*M* Tris HCl, pH 7.5, 12 m*M* $MgCl_2$, at 17.8°C. Adapted from Ref. 25.

ence ΔG_{dock} between the two structurally defined minima in the folding free energy landscape of the hairpin ribozyme is calculated from $-RT \ln(K_{dock})$ to −0.34 kcal/mol.[25] We find that mutations, changes in metal ion concentration, and the nature of the helical junction between domains A and B strongly impact the equilibrium distribution between docked and extended conformers.

For example, linking the wild-type substrate to the ribozyme through a 6-nucleotide bulge additionally stabilizes the docked conformer by 0.28 kcal/mol,[25] consistent with previous observations that bulges impose bends into RNA helical junctions.[65] The natural four-way junction strongly favors formation of the docked complex, leading to an equilibrium in which 95% of the molecules are docked ($\Delta G_{dock} = -1.7$ kcal/mol). The four-way junction also compensates for the loss of specific loop A-loop B interactions; a G+1A substitution or collapsing internal loops A and B into Watson–Crick base-paired helices still leads to 39 and 35% docking, respectively. In fact, 23% docked complex can even be detected in the absence of substrate. In contrast, a perfect three-way junction is found to lead to only 39% docked complex ($\Delta G_{dock} = +0.25$ kcal/mol).[25]

Under physiologic conditions (~1 m*M* Mg^{2+}), the relative enhancement of hairpin ribozyme docking by the four-way junction is still more dramatic. Here, the

two-way junction yields only 8% docked complex, while the four-way junction is characterized by more than 90% docked conformation. Similar for the temperature dependence: The four-way junction favors docking at significantly higher temperatures than does the two-way junction.[25] This higher tertiary structure stability of the naturally occurring four-way junction hairpin ribozyme is the result of a lower entropic cost of docking,[66] and may play an important role for folding and function of the ribozyme in vivo.

Re-ligation of previously cleaved RNA is an important step in rolling-circle replication of satellite RNA in vivo, and requires assembly of a ternary ribozyme–product complex for *trans* reactions in vitro. In the presence of saturating concentrations of nonligatable cleavage product analogs, tr-FRET reveals the global structures of the extended and docked conformations and their equilibrium position to be virtually identical to those in the presence of substrate.[25] This observation indicates that neither the global structure nor the thermodynamic stability of the docked conformation change significantly upon cleavage, explaining the easy reversibility of cleavage.

In summary, our results prove tr-FRET to be an elegant tool to study the free energy landscape associated with folding of the hairpin ribozyme from a defined intermediate to a native conformer. The flexibility of the molecule is revealed and the measured intramolecular distances may serve as constraints in molecular modeling of the underlying global RNA architecture.[35] However, the large-scale conformational changes observed by FRET presumably are accompanied by local structural changes. To study their kinetics, a fluorescence probe sensitive to local structural rearrangements is desirable. We found 2-aminopurine to provide for such a probe.

Local Structural Dynamics in the Catalytic Core is Observed by 2-Aminopurine Fluorescence

The adenosine analog 2-aminopurine (AP) is a strongly fluorescent base (excitation: 320 nm; emission: 360 nm; quantum yield: 68%) and can be selectively excited in the presence of the naturally occurring nucleobases, which maximally absorb around 260 nm.[58,67] AP (ribo)nucleotide can be directly incorporated into a synthetic RNA chain, where it base pairs with uracil and is very sensitive to local π–π stacking interactions with surrounding nucleobases. Stacking interactions with the natural nucleobases generally quench the AP fluorescence,[68] making it a good probe of changes in those local interactions. To monitor structural changes in the catalytic core of the hairpin ribozyme, we have incorporated commercially available 2′-O-methylated AP ribonucleotide into positions −1, +1, or +2 of noncleavable substrate analog S(dA-1), and monitored temporal changes in AP steady-state fluorescence upon addition of a threefold excess of ribozyme under standard conditions.[63] Figure 4 illustrates our results. A G+1AP mutant substrate analog does not lead to any fluorescence change, as this modification interferes with both docking and cleavage activity of the hairpin ribozyme, similar to the G+1A mutation (see section on domain docking above). The A-1AP mutant substrate analog shows a slight fluorescence decrease upon docking of its ribozyme–substrate complex. By far the most significant fluorescence change is observed upon docking of the U+2AP substrate analog, in which case the fluorescence increases more than two-fold, consistent with substantial unstacking of the AP base. The kinetics of this local unstacking event is biphasic and yields very similar rate constants as global docking of this ribozyme–substrate analog complex when observed by ss-FRET (Figure 4). This observation suggests that global domain docking, as observed by ss-FRET, is coupled to a local structural rearrangement around position +2, as detected by AP fluorescence.

To further test whether AP+2 unstacking and domain docking are directly linked, we have studied the kinetics of the AP+2 fluorescence change over a wide range of Mg^{2+} concentrations from 2 to 200 m*M*.[63] Throughout this range, the fast-phase rate constant increases with the Mg^{2+} concentration and matches that for global domain docking, suggesting that AP+2 unstacking is the results of an induced fit between substrate and ribozyme upon domain docking. This provides direct evidence for quasi-hierarchical folding of the hairpin ribozyme.[21] The slow-phase rate constant is Mg^{2+} independent, possibly an indication that the associated process may not be electrostatically driven, unlike domain docking.

What precisely is the conformational rearrangement that AP undergoes in position +2? AP fluorescence has a number of properties that can be used to approach this question. Previously, it has been shown that AP incorporated into a nucleic acid chain exhibits four distinct fluorescence lifetimes that represent different base-stacking states;[69] the longest lifetime, typically around 10 ns and yielding the highest steady-state fluorescence signal, is indicative of a completely unstacked base; the shortest lifetime (typically 50–90 ps) reflects a strongly stacked and quenched AP; and the two intermediate lifetimes represent bases in the population with partial stacking interactions. We find

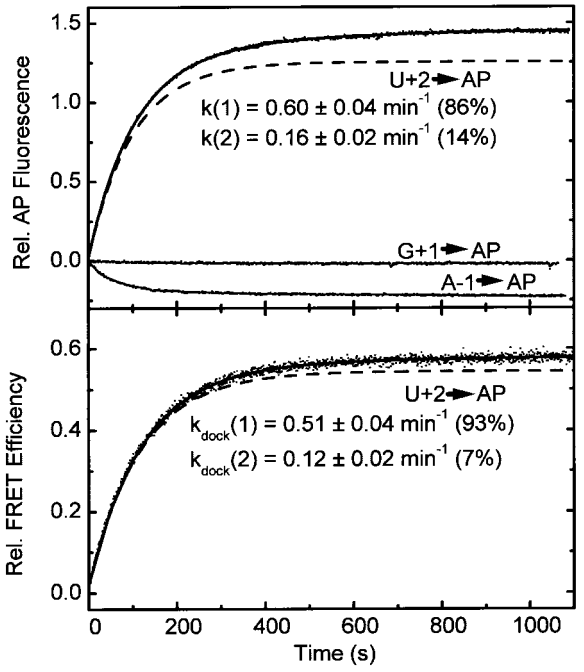

FIGURE 4 Analysis of the local structural change involving substrate position +2 of the hairpin ribozyme under standard conditions (50 m*M* Tris HCl, pH 7.5, 12 m*M* $MgCl_2$, at 25°C). (a) Change of AP steady-state fluorescence upon docking. After formation of the ribozyme–substrate complex (containing noncleavable substrate analogs with AP in either the −1, +1, or +2 position), the relative change in AP fluorescence is observed; only the U+2AP substrate leads to a significant change that is best fit to a double-exponential growth function with the indicated rate constants (with errors from comparing three independent determinations) and relative amplitudes. Dashed line, contribution of the fast-phase component alone. (b) Analysis of the docking kinetics of U+2AP mutant ribozyme–substrate complex by ss-FRET. After formation of the ribozyme–substrate complex (containing noncleavable substrate analog) under standard conditions, the relative FRET efficiency between the domain terminal fluorophore pair increases as a result of domain docking. The data are best fit to a double-exponential growth function (solid line)[24] with the indicated rate constants (with errors from comparing three independent determinations) and relative amplitudes. Dashed line, contribution of the fast-phase component alone. Adapted from Ref. 63.

that the steady-state fluorescence increase observed for the U+2AP substrate analog is due to a substantial fractional increase of the longest lifetime component,[63] further corroborating the notion that AP in position +2 unstacks upon domain docking.

The fluorescence anisotropy decay of AP directly reports on the motion of the base. The decay can be caused by both local rotation of the base, which occurs on the subnanosecond time scale, and overall rotational diffusion of the complex in which the base is incorporated, typically of a nanosecond time scale.[69] We therefore have compared the fluorescence anisotropy decay of the U+2AP mutant ribozyme–substrate analog complex in the absence and presence of Mg^{2+} (i.e., before and after docking, respectively) and have found that a fast-decay component of 420 ps is lost upon domain docking.[63] We therefore conclude that the local motion of AP in position +2 becomes restricted upon domain docking, so that its fluorescence anisotropy can only decay through the slow overall rotational diffusion pathway.

How can these observations be explained in the context of the recent crystal structure of the hairpin ribozyme?[37] Figure 1b shows details of the catalytic core structure. As discussed above, the G+1:C25 interaction is a crucial anchor point between the two domains. It is possible only if G+1 flips out of domain A and docks into a highly complementary binding pocket in the minor (shallow) groove of domain B (Figure 1a). This conformational rearrangement leads to complete unstacking of the +2 position nucleobase from G+1 (Figure 1b), explaining the observed steady-state and time-resolved fluorescence changes when this position is occupied with AP. Our data therefore demonstrate that G+1 flipping and domain docking occur concomitantly, providing direct evi-

dence for an induced fit of the two RNA domains when engaging in a functional complex, consistent with uv cross-linking results.[70]

The final question we have to address is why cleavage of substrates mutated at position +2 is slower than that of the U+2 wild-type substrate. U+2 is preferred, yet not absolutely required for cleavage, as all mutants (including modification to an abasic site) still result in significant cleavage activity.[63] In the crystal structure, U+2 points away from the cleavage site (Figure 1b), making a single hydrogen bond with G+8, which has been implicated in acting as a general base (or possibly acid) catalyst.[64] Hence, it is unlikely that U+2 plays a direct role in reaction chemistry, and its mutation most likely interferes with proper positioning of G+8. Our tr-FRET data suggest that U+2 substitutions stabilize a docked conformation; our AP fluorescence data suggest that the AP+2 base unstacks from G+1, as seen for U+2 in the crystal structure, and becomes restricted in its structural dynamics. tr-FRET and hydroxyl-radical footprinting data indicate that the docked conformer of the mutant ribozyme–substrate complexes has the same interdomain distance and specific solvent-inaccessible core as that of the wild-type complex, i.e., it is native-like.[63] A plausible explanation for these observations is that bases substituting U+2 establish additional interactions that stabilize a native-like conformation, yet have to be broken for the complex to proceed to the chemical transition state. Only a uracil in position +2 makes the correct contacts (for example to G+8) and/or avoids incorrect contacts that lead to a kinetic trap. Consistent with this model, the additional stabilization energy measured by tr-FRET for the docked conformer of a U+2G mutant substrate is of the same magnitude as its additional transition state enthalpy (0.5 kcal/mol).[63]

THE HDV RIBOZYME

HDV is a small satellite of the hepatitis B virus (HBV). HDV is an infectious human pathogen that, upon coinfection with HBV, results in intensification of disease symptoms associated with hepatitis, such as liver cirrhosis.[71] Both the circular HDV RNA genome and its complementary antigenome contain the same *cis*-cleaving, ~85 nucleotide catalytic RNA motif. The sequences of these two forms of the HDV ribozyme are ~75% identical, and they share a secondary structure comprising the five helices P1, P1.1, P2, P3, and P4, intertwined in a nested double pseudoknot (Figure 5a).[71,72] The HDV ribozyme is the only known catalytic RNA associated with an animal virus, yet it has the same function in double-rolling circle replication of HDV RNA as the other small ribozymes isolated from satellite RNAs of plants and fungi.

Both *cis*- and *trans*-cleaving derivatives of the HDV ribozyme have been used to study the interplay of structure and function in this catalytic RNA. For example, cross-linking studies on a *trans*-acting version showed that introduction of a photoreactive azidophenacyl group at the cleavage site results in specific cross-links to the joining sequence between P4 and P2 (J4/2), and to the 3′ sides of P3 and its closing loop L3.[73] These results correlate well with hydroxyl radical footprinting data, which indicate that these regions become solvent inaccessible when the HDV ribozyme is folded in the presence of millimolar Mg^{2+} concentrations.[73] Taken together these data suggest the formation of a compact tertiary structure that places the cleavage site phosphate deep within an active site cleft that is surrounded by nucleotides previously found to be functionally important.[72]

The crystal structure of the 3′ product of a *cis*-acting form of the genomic ribozyme, engineered to bind to the small RNA-binding U1A protein, has provided a good platform to rationalize these and other biochemical data.[74] Its overall secondary structure and base-pair interactions are summarized in the inset of Figure 5a, with details of the catalytic core in Figure 5b. Recent studies have revealed that the HDV ribozyme has the ability to cleave in the presence of monovalent metal ions alone, albeit with significantly reduced activity.[46] This observation, as for the hairpin ribozyme, implies that the RNA chain contains all necessary components for cleavage and exactly positions them in the catalytic core for reaction chemistry to occur. The crystal structure of the 3′ product shows the O2 and N3 of a specific cytosine, C75 (C76 in the antigenomic form), within hydrogen-bonding distance of the 5′ leaving group, suggesting that this nucleobase may play an active role in catalysis.[74] Indeed, a C76A mutation in the antigenomic form results in pK_a changes of the self-cleavage reaction that are consistent with this nucleotide acting as a general base catalyst.[75] However, the inverted pH dependence of self-cleavage by the genomic ribozyme in the presence of monovalent metal ions supports a mechanism in which C75/76 acts instead as a general acid catalyst.[46] Although the latter observation might alternatively be explained by the pH susceptibility of a three-nucleotide motif unique to the genomic sequence,[76] there is little doubt that the HDV ribozyme, like the other small ribozymes, is an example of the growing number of catalytic RNAs in which an RNA side chain actively contributes to transition state chemistry.[12,77,78] Studies of the folding pathway of

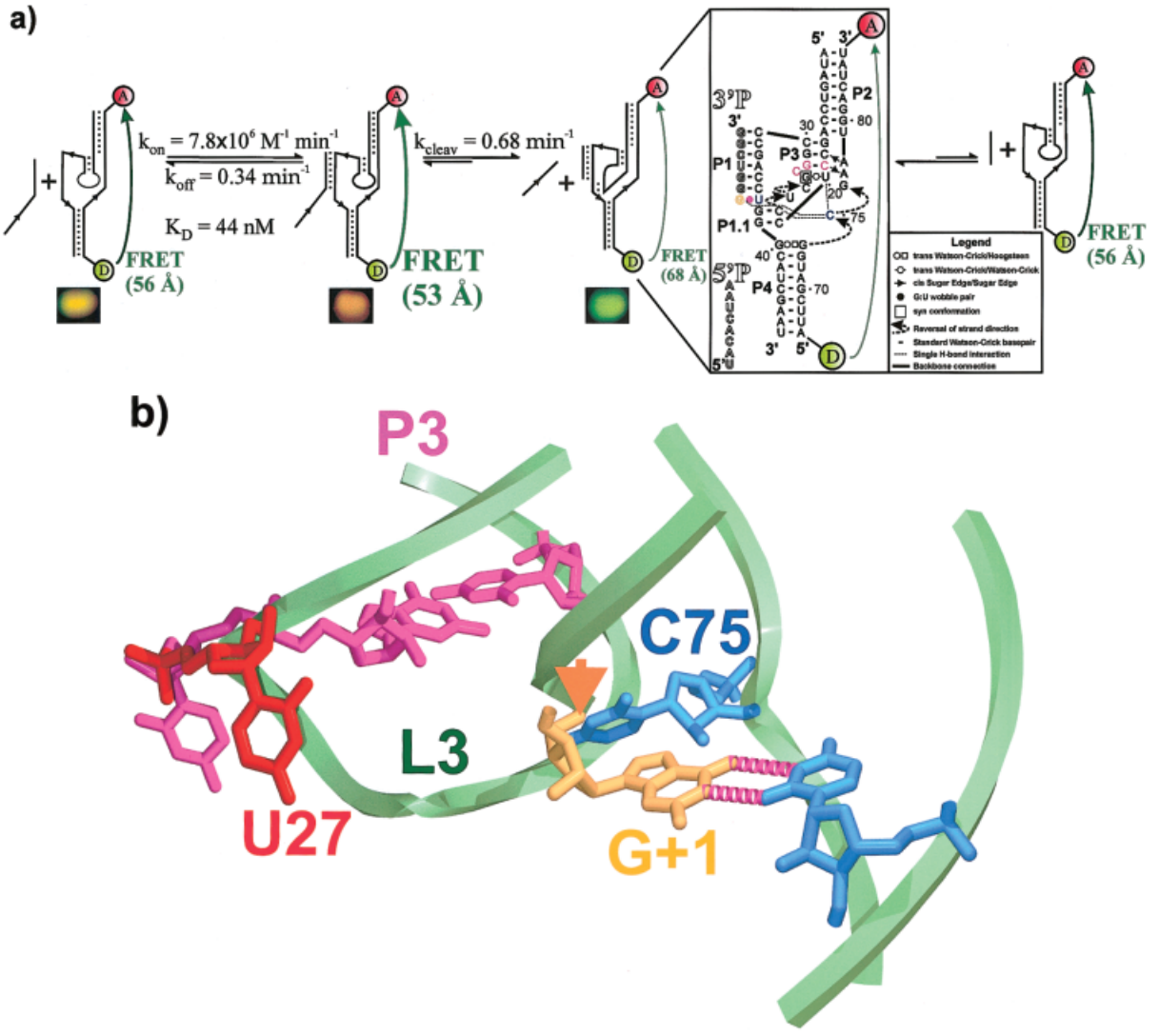

FIGURE 5 Catalysis by the HDV ribozyme. (a) Schematic of the minimal reaction pathway of the *trans*-acting HDV ribozyme as refined by our FRET studies. Reversible substrate binding and formation of helix P1 causes the ribozyme complex to become slightly more compact; FRET (green arrow) between a terminal donor (D) and acceptor (A) fluorophore pair increases (indicative of a fluorophore distance decrease from 56 to 53 Å) and we observe a single red-shifted band on a FRET gel-shift assay (shown below the schematic of each complex). After catalysis, the 5′ product is released (with no observable re-ligation) and the overall structure of the ribozyme–3′ product complex becomes significantly extended (to 68 Å) as evidenced by a decrease in FRET and a green-shifted FRET gel-shift band. This ribozyme–3′ product complex models the postcleavage crystal structure[74] (inset: two-dimensional representation of our construct with its 5′ and 3′ products (5′P, 3′P), shown with a tertiary structure annotation according to Ref. 85 as expected from the crystal structure; the colored nucleotides and wobble pair interaction are the ones detailed in (b). Slow 3′ product release allows the ribozyme to regenerate and undergo another catalytic cycle. The indicated rate and equilibrium constants were measured in 40 m*M* Tris HCl, pH 7.5, 11 m*M* $MgCl_2$, at 25°C. Adapted from Ref.80. (b) Details of the catalytic core in the postcleavage structure. G+1 is held in place by a two-hydrogen-bond wobble interaction (dashed tubes) with U37 so that the cleavage site (arrow) becomes exposed to C75, the potential general acid or base catalyst. U27, a unique insert found in loop L3 of the crystallized genomic form of the HDV ribozyme (not present in our original construct shown in (a), unstacks from helix P3 and the adjacent C26 (green ribbon, backbone). This figure was generated using the 3′ product crystal structure[74] and Swiss-PdbViewer 3.7.[86]

the HDV ribozyme will reveal how this catalytic RNA is able to position the essential reaction components to accomplish site-specific chemistry.

Up to now, in the absence of information on any conformational changes, the prevalent assumption has been that the precursor, transition state, and cleaved structures are all alike.[74,79] To test this assumption, we have applied our array of ss-FRET, tr-FRET, and AP fluorescence assays to probe for global and local structural rearrangements on the reaction pathway of the *trans*-acting HDV ribozyme. We have found evidence for surprisingly large conformational changes that are summarized in Figure 5a and reviewed below.

A Global Structural Transition Upon Cleavage of the *trans*-Acting HDV Ribozyme is Revealed by Steady-State FRET

To allow for attachment of fluorescein and tetramethylrhodamine as donor–acceptor pair to the ends of helices P4 and P2, respectively, we have separated the HDV ribozyme into three synthetically accessible RNA strands, two ribozyme strands, and an external substrate, as indicated in Figure 5a. The RNA sequences are a hybrid between the genomic and antigenomic forms of the HDV ribozyme, and were derived after screening a number of variants for optimal activity. By annealing at least a twofold excess of the unlabeled strand to the labeled one, a catalytically active ribozyme is formed that cleaves substrate S3 at a rate constant of 0.68 min^{-1} under standard conditions (40 m*M* Tris HCl, pH 7.5, 11 m*M* $MgCl_2$, at 25°C). This catalytic activity compares well with previously characterized *trans*-acting HDV ribozymes. Together with similar metal ion, temperature, and pH dependencies, this establishes our three-strand ribozyme as a suitable model system to study folding of the HDV ribozyme into a functional structure.[80]

To investigate conformational changes upon substrate binding, we employ a noncleavable S3 substrate analog, ncS3, with a 2′O-methyl modification at the cleavage site to block reaction chemistry. When this substrate is added to the assembled ribozyme in saturating excess, a 9% increase in relative FRET efficiency is observed as the result of precursor complex formation (Figure 6a). The pseudo-first order rate constant for this increase is linearly dependent on the excess concentration of ncS3, indicating that the observed FRET increase is a direct result of substrate binding. From this dependence we are able to extract a second-order substrate binding rate constant k_{on} of $7.8 \times 10^6 M^{-1}min^{-1}$, within threefold of a value previously measured for a related HDV ribozyme–substrate complex.[81] When instead the cleavable substrate S3 is added, we observe a slight initial increase and subsequent significant decrease by 26% in relative FRET efficiency (Figure 6a). The rate constant of the latter FRET decrease is similar (0.50 min^{-1}) to the cleavage rate constant obtained using radioactive assays.[80] These observations are consistent with the notions that (1) the substrate (precursor) complex is slightly more compact than the free ribozyme, leading to a slight FRET increase upon substrate binding; and (2) that the complex becomes significantly extended upon cleavage and product complex formation, yielding a strong FRET decrease.

To further test this hypothesis we directly initiated the formation of the product complex by adding only the 3′ segment of the substrate (5′-GGGUCGG-3′, termed 3′P, Figure 5a) to the ribozyme. It has been shown previously that this 3′ segment stays bound to the ribozyme after cleavage, while the 5′ segment rapidly dissociates.[81] Indeed, upon addition of 3−P to the ribozyme the relative FRET efficiency rapidly decreases by 33%, indicating the formation of an extended product complex (Figure 6a). A FRET decrease by 33% upon direct formation of the product complex compared to 26% upon binding and cleavage of substrate is consistent with the fact that typically ~77% of substrate is cleaved and converted to product complex under these conditions.[80]

We also have used 3′P as a chase to measure the dissociation rate constant of ncS3. To this end, we first form the ribozyme–ncS3 complex, then add a micromolar excess of 3′P. We observe a single-exponential FRET decrease. Its rate constant $k_{off} = 0.34$ min^{-1} is independent of the concentration of 3′P, indicating that our chase concentration is sufficient, and that active displacement (i.e., a promotion of substrate dissociation) by the chase does not take place.[82] This substrate dissociation rate constant is within fourfold of a previously reported value for another *trans*-acting HDV ribozyme,[81] and together with the substrate binding rate constant k_{on}, defines the equilibrium dissociation constant $K_D = k_{off}/k_{on}$ as 44 n*M*. Conversely, the 3′ product cannot be chased off its complex, even when utilizing up to a 5 μM excess of ncS3 as chase, indicating its significantly higher binding affinity, as previously observed.[81]

One feature of ss-FRET measurements in bulk solution is that they average over all molecule conformations present. To test for the homogeneity of our preparations and further confirm that the ribozyme–substrate and –product complexes are indeed structurally distinct, we have developed a FRET gel mobility assay similar to one used to characterize protein–nucleic acid interactions.[83] Ribozyme alone and in

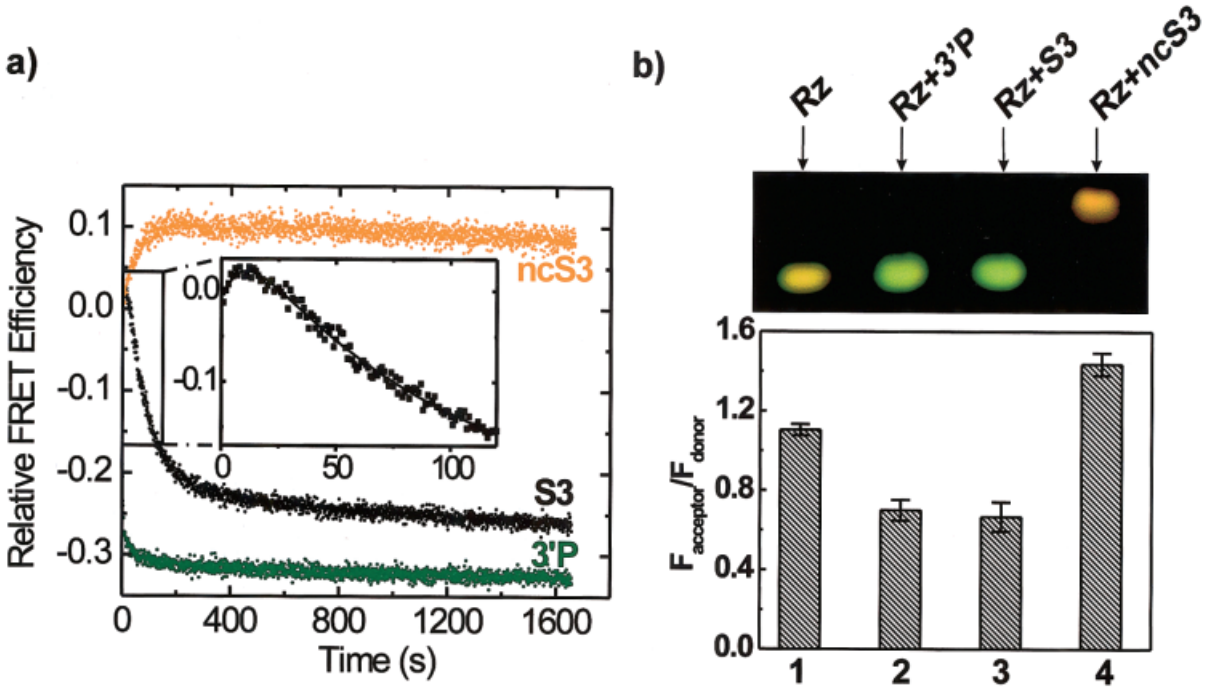

FIGURE 6 Steady-state FRET studies using 50 n*M* of fluorescein–tetramethylrhodamine labeled *trans*-acting HDV ribozyme in 40 m*M* Tris HCl pH 7.5, 11 m*M* $MgCl_2$, 25 m*M* DTT, at 25°C. (a) Change over time in the relative FRET efficiency of the doubly labeled ribozyme upon addition of 250 n*M* noncleavable substrate analog (ncS3), cleavable substrate (S3), or 3′ product (3′P), as indicated. Inset: The data set for S3, after a short initial increase, gives an exponential decrease that pertains to substrate cleavage (solid line; rate constant: 0.50 min^{-1}). (b) Nondenaturing polyacrylamide gel electrophoresis of fluorescein-tetramethylrhodamine doubly labeled complexes. The free ribozyme (Rz) comigrates with the ribozyme–3′ product complex (Rz+3′P, upper panel), but can be distinguished by its ratio of acceptor:donor fluorescence (lower panel; error bars are derived from three gel runs). The ribozyme–substrate complex (Rz+S3) undergoes catalysis and is observed as the ribozyme–3′ product complex, while the ribozyme–noncleavable substrate analog complex (Rz+ncS3) stays intact, migrating slower with a higher acceptor:donor fluorescence ratio. Adapted from Ref. 80.

complex with S3, ncS3, and 3'P is electrophoresed on a nondenaturing polyacrylamide gel. The gel is then scanned with 488 nm light from a laser and the fluorescence emission F is observed at two different wavelength ranges, around 530 nm for the fluorescein donor and >610 nm for the tetramethylrhodamine acceptor. A relative FRET efficiency for a band in the gel is calculated as $F_{acceptor}/F_{donor}$, and, defining F_{donor} as green and $F_{acceptor}$ as red, the image in Figure 6b was generated.[80] We find that the free ribozyme (Rz) as well as its complexes with 3′P and ncS3 migrate as homogeneous single bands, with any alternate bands contributing less than 15% of the intensity of the major ones. Lane 1, loaded with the free ribozyme, shows a band with intermediate acceptor-to-donor (FRET) ratio (Figure 6b, lower panel), consistent with our solution measurements. Its band comigrates with the ribozyme–3′P complex in lane 2, which shows a decreased FRET ratio (or "green-shifted", i.e., donor-fluorescence dominated band). Lane 4, loaded with the ribozyme–ncS3 complex, shows a band with increased FRET ratio ("red-shifted") and lower mobility, also consistent with the solution measurements. These findings further support the existence of structurally distinct pre- and postcleavage ribozyme complexes.

Lane 3, loaded with the ribozyme-cleavable substrate complex (Rz+S3), shows a band identical in color and mobility to the one in lane 2 (Figure 6b), suggesting that the substrate has largely been cleaved and converted into ribozyme-bound 3′ product. The result is similar when the ribozyme is first run into the gel for 2 h, followed by the faster migrating substrate so that the ribozyme–substrate complex can only form and cleave in the gel (data not shown). These observations provide evidence that cleavage of substrate S3

Table I Fluorescence Properties of Fluorescein (Donor) and Tetramethylrhodamine (Acceptor) Labeled Ribozyme Constructs[a]

Parameter	Rz	Rz+ncS3	Rz+3′P
Mean donor lifetime without acceptor (ns)	4.11 ± 0.05	4.18 ± 0.05	3.93 ± 0.05
Mean donor–acceptor distance (Å)	56 ± 1	53 ± 1	68 ± 1
fwhm (Å)	25 ± 1	19 ± 1	27 ± 1
χ^2	1.36	1.43	1.48
Anisotropy donor	0.013 ± 0.003	0.013 ± 0.003	0.013 ± 0.003
Anisotropy acceptor	0.021 ± 0.003	0.024 ± 0.003	0.022 ± 0.003

[a] Values are from Ref. 80; fwhm, full-width-at-half-maximum; χ^2, reduced chi-square.

occurs within the native gel—hence, our ribozyme–substrate complex is catalytically active.

Our results demonstrate conformational dynamics of the *trans*-acting HDV ribozyme along its reaction pathway (Figure 5a). Upon substrate binding a slight structural compaction is observed. This is followed by a substantial extension as cleavage occurs. The latter conformational change is related to the catalytic RNA achieving its transition state, which begs the question of whether the transition state structure resembles more that of the precursor or the ribozyme–3′ product complex.

There is strong evidence from pH titration experiments that C75/76 deprotonates the 2′ hydroxyl nucleophile[75] and/or protonates the 5′ oxyanion leaving group in the rate-limiting step (i.e., in the transition state) of phosphodiester transfer.[46,76,77] In the 3′ product crystal structure, O2 and N3 of C75/76 are within hydrogen-bonding distance to the 5′ OH leaving group.[12,74] Therefore, it is plausible that a C75/76-5′OH hydrogen bond, or a similar interaction, is also present in the transition state, juxtaposing the catalytic base and the scissile phosphate. Given that the substrate and product complexes are structurally distinct, as directly observed here by ss-FRET, we have proposed that the transition state in HDV ribozyme catalysis is closer in structure to, although not necessarily identical with, the product complex.[80] We speculate that our capture of significant structural change along the reaction trajectory may present the structural basis of the recently described utilization of intrinsic substrate binding energy to the overall catalytic rate enhancement by the *trans*-acting HDV ribozyme.[84]

Whereas ss-FRET has revealed the existence and kinetics of global conformational changes of the HDV ribozyme, tr-FRET allows for the extraction of absolute donor–acceptor fluorophore distances, as discussed in the following.

The Global Geometries of Precursor and Product Forms are Derived from Time-Resolved FRET

While our analyses of acceptor-to-donor fluorescence ratios reveal qualitative changes in fluorophore distance, we also sought to quantify the underlying RNA structural changes. We therefore have analyzed the time-resolved donor (fluorescein) decay curves for the ribozyme alone (Rz), the ribozyme–noncleavable substrate analog complex (Rz+ncS3), and the ribozyme–3′ product complex (Rz+3′P), each of them singly labeled with donor, as well as doubly labeled with donor and acceptor. The decay curves of the three donor-only labeled complexes virtually superimpose and yield similar mean lifetimes of approximately 4 ns (Table I).[80] The donor fluorescence decays of all three donor–acceptor doubly labeled complexes are faster, indicative of FRET between donor and acceptor. The anisotropies of the fluorophores in all complexes are low and only slightly vary between the different complexes (Table I), suggesting that both donor and acceptor can freely rotate. Under this assumption and using Förster theory, the fluorophore distance distributions are analyzed as described in the section on global geometry and equilibrium position, yielding mean donor–acceptor distances of 56 Å (full-width-at-half-maximum, fwhm: 25 Å) for the ribozyme; 53 Å (fwhm: 19 Å) for the ribozyme–ncS3 complex; and 68 Å (fwhm: 27 Å) for the ribozyme–3′P complex (Table I). In all three cases, a single distance distribution fits the decay data well, as judged by the residuals and the reduced χ^2 values ($<$1.5, Table I); introducing a second distance distribution does not improve the fits, indicating a high structural homogeneity of our RNA preparations. These time-resolved FRET data directly support our steady-state fluorescence measurements (see section immediately above) in that the substrate complex is slightly more compact (by ~3Å) than the free ri-

bozyme, yet becomes significantly extended (by ~15 Å) upon cleavage and product complex formation (Figure 5a).[80] Interestingly, the full-width-at-half-maximum of these complexes, which is a measure of their structural flexibility, suggests that a relatively rigid structure is acquired prior to cleavage whereas the postcleavage complex adopts a more flexible conformation.

The fluorophore distance measured for our ribozyme–3′P complex (68 Å) can directly be compared to an analogous distance of 74 Å between helices P2 and P4 in the crystal structure of the self-cleaved genomic form of the HDV ribozyme.[74] Considering the fact that the crystallized construct contains an artificial U1A-protein binding loop to close helix P4, these distances are in good agreement. Our measurements for the free ribozyme and the substrate-bound precursor lack such values from high resolution structures to compare with. However, our discovery of significant global conformational change along the HDV ribozyme reaction pathway (Figure 5a)[80] raises the question of whether local structural transitions also occur. FRET does not allow us to directly detect such transitions since the donor–acceptor probes are positioned far from the catalytic core. Therefore, we have begun to utilize 2-aminopurine as a local fluorescent probe to provide such information.

Local Structural Dynamics upon Cleavage is Observed by AP Fluorescence

To complement our FRET measurements that reveal global conformational changes of the HDV ribozyme, we have started to examine localized conformational transitions by fluorescence quenching of AP ribonucleotide inserted into position 27 of our three-strand ribozyme construct (see also section on local structural dynamics above). This choice is based on the proximity of position 27 to the catalytic core of the genomic form of the HDV ribozyme (Figure 5b) and on the fact that U27 in the genomic form is tolerated without loss of cleavage activity compared to the antigenomic form that lacks this insertion.[72]

Similar to our ss-FRET assays (see section on global structural transition above), AP27 fluorescence changes are monitored over time upon addition of saturating concentrations of the noncleavable substrate analog S3 (ncS3), cleavable substrate (S3), or 3′ product (3′P) (Figure 7). Our results are consistent with the findings from our ss-FRET experiments in that they reveal not only globally but also locally distinct pre- and postcleavage conformations. In particular, a slight decrease in AP fluorescence is observed upon binding of ncS3, indicating formation or stabilization of local stacking interactions between AP27 and neighboring nucleobases in the complex. By contrast, a significant increase in AP fluorescence occurs upon binding of 3′P, indicative of AP unstacking (see section on local structural dynamics above). This observation is consistent with the 3′ product crystal structure in which position 27 is extruded from the stack of helix P3 (Figure 5b).[74] Finally, when cleavable substrate S3 is added to the ribozyme, a subtle decrease is followed by a substantial increase in AP fluorescence. This pattern suggests that the substrate binds and is subsequently cleaved, leading to initial stacking in the ribozyme–substrate and unstacking in the ribozyme–3′ product complex. Our data demonstrate that local structural rearrangements near the catalytic core occur upon substrate binding and cleavage.

It is difficult to model the substrate sequence 5′ of the cleavage site extending out of the catalytic core of the postcleavage crystal structure without sterical clash. This raises the idea that the 5′ extension may be involved in the local structural rearrangement reported by AP fluorescence. One of several possible explanations for the structural difference between the substrate and product complexes then is that helix P1.1, which forms the bottom of the catalytic cleft, is absent in the substrate complex to accommodate the substrate 5′ extension, as suggested in Figure 5a. AP as a fluorescent probe reveals such subtle localized dynamics in the HDV ribozyme that cannot be detected by FRET.

The slow time course of S3 substrate cleavage in Figure 7 reveals that insertion of AP in position 27 of the HDV ribozyme leads to a 170-fold reduced cleavage rate. Ideally, a modification within the ribozyme used to report on conformational changes should not so drastically affect the rate of cleavage. In this particular case, AP27 probably forms a Watson–Crick base pair with U20; such a base pair is expected to stack on helix P3 in place of the G25:U20 *trans*-Watson–Crick base pair shown in Figure 5a. This local structure would be consistent with the strong fluorescence quenching observed in the AP27 modified ribozyme–substrate complex. Apparently, AP27 stacking interactions have to be broken to proceed to catalysis and formation of the ribozyme–3′ product complex, in which AP27 is strongly unquenched and hence unstacked. The necessary breaking of favorable AP27 stacking (and possibly hydrogen-bonding) interactions would explain the slower cleavage rate upon introduction of this modification, an example for a kinetic RNA folding trap. We are currently explor-

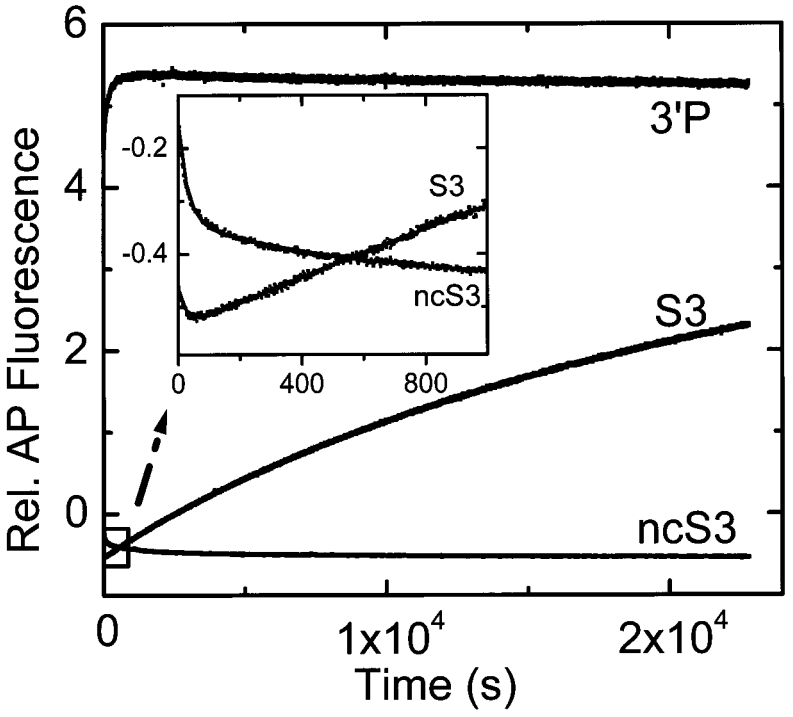

FIGURE 7 Change over time of AP steady-state fluorescence in position 27 of 400 n*M trans*-acting HDV ribozyme upon addition of 1200 n*M* 3′ product (3′P), cleavable substrate (S3), or noncleavable substrate analog (ncS3), as indicated. Inset: Blow-up of the data sets for S3 and ncS3, emphasizing the initial decrease and subsequent increase of the former data set. Standard conditions: 40 m*M* Tris HCl, pH 7.5, 11 m*M* $MgCl_2$, at 25°C.

ing other modification sites to monitor local structural transitions in the HDV ribozyme.

CONCLUSIONS

We have made use of fluorescence resonance energy transfer and 2-aminopurine quenching to highlight global and local conformational changes, respectively, in small catalytic RNAs such as the hairpin and HDV ribozymes. These RNA enzymes precisely position reaction components for site-specific organic chemistry, which requires folding into a particular three-dimensional structure. Both their folding and catalytic activity make use of the dynamic nature of an RNA structure, which typically is characterized by a rugged folding free energy landscape. Fluorescence techniques explore these landscapes and provide kinetic and thermodynamic information. Further developments in RNA synthesis and labeling and fluorescence spectroscopic equipment (including that for single-molecule experiments) will broaden the application of the concepts described herein to other RNAs. The more RNA systems are studied this way, the better we will understand the physicochemical principles that govern the function of this ubiquitous biopolymer.

The authors wish to thank Neocles Leontis for help with the structure annotations in Figures 1a and 5, and Diane Hannemann for her work on the 2-aminopurine modified HDV ribozyme. This work was supported by NIH grant GM62357, and startup funds from the University of Michigan to NGW, a Rackham Merit predoctoral fellowship and NIH Molecular Biophysics Training Grant to DAH, and a postdoctoral fellowship from the Swiss National Fonds to DR.

REFERENCES

1. Gesteland, R. F.; Cech, T. R.; Atkins, J. F. E. The RNA World, 2nd ed.; Cold Spring Harbor Laboratory Press: Cold Spring Harbor, NY, 1999.
2. Schultes, E. A.; Bartel, D. P. Science 2000, 289, 448–452.
3. Nissen, P.; Hansen, J.; Ban, N.; Moore, P. B.; Steitz, T. A. Science 2000, 289, 920–930.
4. Valadkhan, S.; Manley, J. L. Nature 2001, 413, 701–707.

5. Noller, H. F.; Hoffarth, V.; Zimniak, L. Science 1992, 256, 1416–1419.
6. Wilson, K. S.; Noller, H. F. Cell 1998, 92, 337–349.
7. Staley, J. P.; Guthrie, C. Cell 1998, 92, 315–326.
8. Jaschke, A. Curr Opin Struct Biol 2001, 11, 321–326.
9. Limbach, P. A.; Crain, P. F.; McCloskey, J. A. Nucleic Acids Res 1994, 22, 2183–2196.
10. Agris, P. F. Prog Nucleic Acid Res Mol Biol 1996, 53, 79–129.
11. Narlikar, G. J.; Herschlag, D. Ann Rev Biochem 1997, 66, 19–59.
12. Shih, I. H.; Been, M. D. Ann Rev Biochem 2002, in press.
13. Doherty, E. A.; Doudna, J. A. Ann Rev Biophys Biomol Struct 2001, 30, 457–475.
14. Hiley, S. L.; Collins, R. A. EMBO J 2001, 20, 5461–5469.
15. Lafontaine, D. A.; Wilson, T. J.; Norman, D. G.; Lilley, D. M. J Mol Biol 2001, 312, 663–674.
16. Salehi-Ashtiani, K.; Szostak, J. W. Nature 2001, 414, 82–84.
17. SantaLucia, J., Jr.; Turner, D. H. Biopolymers 1997, 44, 309–319.
18. Schroeder, S. J.; Burkard, M. E.; Turner, D. H. Biopolymers 1999, 52, 157–167.
19. Brion, P.; Westhof, E. Ann Rev Biophys Biomol Struct 1997,26, 113–137.
20. Tinoco, I., Jr.; Bustamante, C. J Mol Biol 1999, 293, 271–281.
21. Treiber, D. K.; Williamson, J. R. Curr Opin Struct Biol 1999, 9, 339–45.
22. Treiber, D. K.; Williamson, J. R. Curr Opin Struct Biol 2001, 9, 339–345.
23. Thirumalai, D.; Lee, N.; Woodson, S. A.; Klimov, D. Ann Rev Phys Chem 2001, 52, 751–762.
24. Walter, N. G.; Hampel, K. J.; Brown, K. M.; Burke, J. M. EMBO J 1998, 17, 2378–2391.
25. Walter, N. G.; Burke, J. M.; Millar, D. P. Nat Struct Biol 1999, 6, 544–549.
26. Hampel, K. J.; Walter, N. G.; Burke, J. M. Biochemistry 1998, 37, 14672–14682.
27. Walter, N. G.; Burke, J. M. Curr Opin Chem Biol 1998, 2, 24–30.
28. Murchie, A. I.; Thomson, J. B.; Walter, F.; Lilley, D. M. Mol Cell 1998, 1, 873–881.
29. Fedor, M. J. J Mol Biol 2000, 297, 269–291.
30. Welch, P. J.; Barber, J. R.; Wong-Staal, F. Curr Opin Biotechnol 1998, 9, 486–496.
31. Cai, Z.; Tinoco, I., Jr. Biochemistry 1996, 35, 6026–6036.
32. Butcher, S. E.; Allain, F. H.; Feigon, J. Nat Struct Biol 1999, 6, 212–216.
33. Earnshaw, D. J.; Masquida, B.; Muller, S.; Sigurdsson, S. T.; Eckstein, F.; Westhof, E.; Gait, M. J. J Mol Biol 1997, 274, 197–212.
34. Pinard, R.; Heckman, J. E.; Burke, J. M. J Mol Biol 1999, 274, 197–212.
35. Pinard, R.; Lambert, D.; Heckman, J. E.; Esteban, J. A.; Gundlach, C. W.; Hampel, K. J.; Glick, G. D.; Walter, N. G.; Major, F.; Burke, J. M. J Mol Biol 2001, 287, 239–251.
36. Pinard, R.; Lambert, D.; Walter, N. G.; Heckman, J. E.; Major, F.; Burke, J. M. Biochemistry 1999, 38, 16035–16039.
37. Rupert, P. B.; Ferre-D'Amare, A. R. Nature 2001,410, 780–786.
38. Chowrira, B. M.; Berzal-Herranz, A.; Keller, C. F.; Burke, J. M. J Biol Chem 1993, 268, 19458–19462.
39. Ryder, S. P.; Strobel, S. A. J Mol Biol 1999, 291, 295–311.
40. Burke, J. M. Nat Struct Biol 2001, 8, 382–384.
41. Hampel, A.; Cowan, J. A. Chem Biol 1997, 4, 513–517.
42. Nesbitt, S.; Hegg, L. A.; Fedor, M. J. Chem Biol 1997, 4, 619–630.
43. Young, K. J.; Gill, F.; Grasby, J. A. Nucleic Acids Res 1997, 25, 3760–3766.
44. Pyle, A. M. Science 1993, 261, 709–714.
45. Murray, J. B.; Seyhan, A. A.; Walter, N. G.; Burke, J. M.; Scott, W. G. Chem Biol 1998, 5, 587–595.
46. Nakano, S.; Chadalavada, D. M.; Bevilacqua, P. C. Science 2000, 287, 1493–1497.
47. Curtis, E. A.; Bartel, D. P. RNA 2001, 7, 546–552.
48. Förster, T. Ann Phys (Leipzig) 1948, 2, 55–75.
49. Stryer, L.; Haugland, R. P. Proc Natl Acad Sci USA 1967, 58, 719–726.
50. Clegg, R. M. Methods Enzymol 1992, 211, 353–388.
51. Wu, P.; Brand, L. Anal Biochem 1994, 218, 1–13.
52. McCarty, R. E. Methods Enzymol 1997, 278, 528–538.
53. Yang, M.; Millar, D. P. Methods Enzymol 1997, 278, 417–444.
54. Lakowicz, J. R. Principles of Fluorescence Spectroscopy, 2nd ed.; Kluwer Academic Publishers: New York, 1999.
55. Selvin, P. R. Nat Struct Biol 2000, 7, 730–734.
56. Lilley, D. M.; Wilson, T. J. Curr Opin Chem Biol 2000, 4, 507–517.
57. Klostermeier, D.; Millar, D. P. Methods 2001, 23, 240–254.
58. Walter, N. G.; Burke, J. M. Methods Enzymol 2000, 317, 409–440.
59. Walter, N. G. Methods 2001, 25, 19–30.
60. Walter, N. G.; Burke, J. M. RNA 1997, 3, 392–404.
61. Bloomfield, V. A.; Crothers, D. M.; Tinoco, I. Nucleic Acids: Structures, Properties, and Functions; University Science Books, Sausalito, CA, 2000.
62. Chowrira, B. M.; Berzal-Herranz, A.; Burke, J. M. Nature 1991, 354, 320–322.
63. Walter, N. G.; Chan, P. A.; Hampel, K. J.; Millar, D. P.; Burke, J. M. Biochemistry 2001, 40, 2580–2587.
64. Pinard, R.; Hampel, K. J.; Heckman, J. E.; Lambert, D.; Chan, P. A.; Major, F.; Burke, J. M. EMBO J 2001, 20, 6434–6442.

65. Zacharias, M.; Hagerman, P. J. J Mol Biol 1995, 247, 486–500.
66. Klostermeier, D.; Millar, D. P. Biochemistry 2000, 39, 12970–12978.
67. Millar, D. P. Curr Opin Struct Biol 1996, 6, 322–326.
68. Jean, J. M.; Hall, K. B. Proc Natl Acad Sci USA 2001, 98, 37–41.
69. Guest, C. R.; Hochstrasser, R. A.; Sowers, L. C.; Millar, D. P. Biochemistry 1991, 30, 3271–3279.
70. Hampel, K. J.; Burke, J. M. Biochemistry 2001, 40, 3723–3729.
71. Hadziyannis, S. J. J Gastroenterol Hepatol 1997, 12, 289–298.
72. Been, M. D.; Wickham, G. S. Eur J Biochem 1997, 247, 741–753.
73. Rosenstein, S. P.; Been, M. D. Biochemistry 1996, 35, 11403–11413.
74. Ferre-D'Amare, A. R.; Zhou, K.; Doudna, J. A. Nature 1998, 395, 567–574.
75. Perrotta, A. T.; Shih, I.; Been, M. D. Science 1999, 286, 123–126.
76. Wadkins, T. S.; Shih, I.; Perrotta, A. T.; Been, M. D. J Mol Biol 2001, 305, 1045–1055.
77. Shih, I. H.; Been, M. D. Proc Natl Acad Sci USA 2001, 98, 1489–1494.
78. Nakano, S.; Proctor, D. J.; Bevilacqua, P. C. Biochemistry 2001, 40, 12022–12038.
79. Ferre-D'Amare, A. R.; Doudna, J. A. J Mol Biol 2000, 295, 541–556.
80. Pereira, M. B.; Harris, D. A.; Rueda, D.; Walter, N. G. Biochemistry 2002, 41, 730–740.
81. Shih, I.; Been, M. D. Biochemistry 2000, 39, 9055–9066.
82. Werner, M.; Uhlenbeck, O. C. Nucleic Acids Res 1995, 23, 2092–2096.
83. Ramirez-Carrozzi, V. R.; Kerppola, T. K. Methods 2001, 25, 31–43.
84. Shih, I.; Been, M. D. EMBO J 2001, 20, 4884–4891.
85. Leontis, N. B.; Westhof, E. RNA 2001, 7, 499–512.
86. Guex, N.; Peitsch, M. C. Electrophoresis 1997, 18, 2714–2723.
87. Zhuang, X.; Kim, H.; Pereira, M. J. B.; Babcock, H. P.; Walter, N. G.; Chu, S. Science 2002, in press.